Title: **Metabolic modeling reveals determinants of synbiotic efficacy in a human intervention trial.**

Authors: Nick Quinn-Bohmann[1] and Sean M. Gibbons[1-4,*]

Affiliations: [1] Institute for Systems Biology, Seattle, WA 98109, USA; [2] Bioengineering Department, University of Washington, Seattle, WA 98195, USA; [3] Genome Sciences Department, University of Washington, Seattle, WA 98195, USA; [4] eScience Institute, University of Washington, Seattle, WA 98195, USA; [*] correspondence addressed to sgibbons@isbscience.org

Abstract

Synbiotic interventions show variable effects across individuals, likely driven by ecological interactions with the endogenous microbiota and the host diet. Rationally predicting individual-specific success or failure of probiotic and prebiotic interventions remains an outstanding challenge. In this study, we leverage microbial community-scale metabolic models (MCMMs) to predict probiotic engraftment and shifts in microbiota-mediated short-chain fatty acid (SCFA) production in response to a synbiotic intervention. Using data from a placebo-controlled synbiotic intervention trial, involving a cocktail of five probiotic strains and the prebiotic inulin, we validate model engraftment predictions with quantitative PCR (qPCR), demonstrating that MCMMs accurately predict probiotic engraftment outcomes in the treatment group with over 85% accuracy. Engraftment varied by species, with *Akkermansia muciniphila* and *Bifidobacterium infantis* displaying higher engraftment rates than *Clostridium beijerinckii, Anaerobutyricum hallii*, and *Clostridium butyricum*. Furthermore, MCMMs predicted significant increases in butyrate and propionate production following synbiotic treatment. MCMM-predicted changes in propionate production in the treatment group were negatively associated with changes in C-reactive protein (CRP), a blood marker of systemic inflammation, from baseline to 12 weeks after the synbiotic intervention. Finally, we explore MCMM-predicted responses to a wider range of synbiotic combinations in a larger observational cohort, suggesting that personalized prebiotic selection can augment probiotic efficacy. These findings highlight the potential of metabolic modeling to inform precision microbiome therapeutics.

Introduction

Synbiotics, which combine probiotic microbes with the compounds that these microbes like to eat (i.e., prebiotics), represent a promising avenue for improving the efficacy of microbiome-mediated interventions, targeting everything from prediabetes and autoimmune disorders to neurodegenerative diseases [1–3]. The human colonic microbiota plays a critical role in regulating

host physiology and immunity [4–8]. Probiotic and prebiotic administration have been shown to influence the metabolic outputs of the endogenous microbiota, inhibit pathogen colonization, and enhance mucosal barrier integrity [9,10]. In addition to immunomodulation and supporting metabolic health, emerging evidence suggests that synbiotic interventions may even impact brain function via the gut-brain axis [11–13].

Despite these promising findings, the efficacy of probiotic, prebiotic, and synbiotic interventions can vary significantly between individuals, posing a major challenge for their widespread clinical application [14,15]. Engraftment of a probiotic strain—the ability of the administered microbe to establish and persist within the gut ecosystem—depends on multiple factors, including the availability of a suitable metabolic niche, competitive and cooperative interactions with endogenous microbiota, and interactions with the host immune system [16,17]. Beyond the composition of the commensal microbiota, the interplay between factors like total commensal biomass, propagule pressure (i.e., the probiotic dose), available prebiotic substrates, and host diet can all impact engraftment [18]. In order to rationally predict probiotic engraftment and prebiotic effects across individuals and dietary backgrounds, we require methods that integrate this complexity.

Genome-scale metabolic models (GEMs) provide a powerful mechanistic framework for estimating microbial growth and metabolism [19,20]. Recent advances in constraint-based modeling have extended this approach to diverse microbial communities, yielding microbial community-scale metabolic models (MCMMs) [21]. By integrating genome-scale metabolic reconstructions from hundreds of gut bacterial taxa with flux balance analysis, MCMMs enable predictions of microbe-microbe interactions, competition for resources, and ecosystem-scale metabolic behaviors [21,22]. These models have demonstrated predictive accuracy in estimating microbial growth rates, short-chain fatty acid production, methane production, and metabolic shifts in response to disease status or dietary interventions [21–25]. Notably, prior work has shown that MCMMs can capture the engraftment potential of opportunistic pathogens, such as *Clostridioides difficile*, suggesting that similar approaches could be used to model probiotic engraftment in individual hosts [22,23].

To validate this approach, we aimed to use MCMMs to predict the enrichment of probiotic species based on data from a human intervention trial conducted by Perradeau et al. (2020) [26]. In this double-blind, placebo-controlled intervention trial, participants previously diagnosed with type 2 diabetes mellitus were treated for 12 weeks with either a placebo or a multi-strain synbiotic cocktail (WBF-011). This formulation contained *Akkermansia muciniphila* (AMUC), *Anaerobutyricum hallii* (AHAL), *Bifidobacterium infantis* (BINF), *Clostridium beijerinckii* (CBEI), and *Clostridium butyricum* (CBUT), supplemented with a low-dose of inulin (0.3g), a prebiotic fiber known to support probiotic growth. Participants who received the synbiotic exhibited a significantly greater reduction in the area under the curve (AUC) for glucose during

a standard glucose tolerance test from Week 0 to Week 12, compared to the placebo group, indicating a beneficial population-level effect on glycemic control [26].

Using metagenomic sequencing date, quantitative PCR (qPCR), and immune and metabolic profiling, we assessed the ability of MCMMs to accurately predict probiotic engraftment and the subsequent impact on host metabolism and immune function. Specifically, we evaluated how well MCMM-derived predictions align with observed shifts in microbial composition, metabolite production, and inflammatory markers. Finally, we expand MCMM simulations to a cross-sectional cohort of 156 generally-healthy individuals, to identify personalized prebiotic, dietary, and probiotic interventions that are predicted to maximize individual-specific efficacies of synbiotic interventions. Together, these results provide a promising computational platform for designing personalized synbiotics for human intervention trials.

Results

qPCR shows enrichment of probiotic species in the treatment group

Custom qPCR primer pairs were designed for each of the five probiotic strains in the WBF-011 treatment [26]. Cycle threshold (Ct) values were obtained for all five species in each sample, and were inverted (1/Ct) to serve as a proxy for species abundance. Samples were collected at multiple time points throughout the study, including at baseline (Week 0), during treatment (Week 4), and at the end of treatment (Week 12).

In the placebo group, there were no significant changes in 1/Ct values over time for any of the five probiotic strains (Fig. 1A). In the WBF-011 treatment group, AMUC and BINF exhibited significant enrichment from Week 0 to Week 12 across most participants (Fig. 1B, Mann-Whitney U test, AMUC: $p = 2.7*10^{-7}$; BINF: $p = 4.7*10^{-7}$). At Week 12, the mean 1/Ct for AMUC was 0.033 ± 0.0009, exceeding the species-specific detection threshold of 0.0264, while the mean 1/Ct for BINF was 0.031 ± 0.0004, surpassing its detection threshold of 0.0284. In contrast, CBEI, AHAL, and CBUT showed no comparable enrichment. In nearly all samples, 1/Ct values for these species either remained unchanged or declined after 12 weeks. Generally, these trends suggest that AMUC and BINF probiotics were able to engraft in the majority of individuals included in this study. In the placebo group, enrichment was observed in some samples, though these occurrences were sparse and may have been driven by off-target primer binding to closely related endogenous strains (Fig. 1A).

MCMMs predict species-level enrichment

Models were constructed using Week 0 metagenomic sequencing data from participants in the WBF-011 treatment arm to assess whether MCMMs could predict the engraftment patterns observed in the qPCR results (Fig. 1). For each individual, simulations were run to model the addition of the five probiotic species, assuming a standard European diet, and predicted growth

110 rates were obtained. Growth rates were binarized at a threshold of 0.001 h^{-1}, above which
111 represented growth and below which represented non-growth, and these binary classifications
112 were compared to qPCR-based engraftment thresholds, described above.
113 Across all comparisons (5 predictions for each of 21 samples, total N = 105), model-
114 predicted growth and qPCR results showed 85.7% agreement (Fig. 2A, Cohen's $\kappa = 0.70$,
115 indicating substantial agreement). Perfect agreement was observed in 11 of 21 participants,
116 where all five probiotic engraftment statuses were accurately predicted. Additionally, CBEI was
117 correctly predicted as not growing for all 21 participants, while AHAL had the lowest accuracy,
118 with misclassification in 7 of 21 cases. Overall, there was significant concordance between
119 predictions and observations (Fig. 2B). Across all strains, 57 instances of growth were correctly
120 predicted, 33 instances of non-growth were correctly predicted, 4 cases were incorrectly
121 predicted as growth, and 11 cases were incorrectly predicted as non-growth (Fisher's exact test,
122 $p = 1.3 \times 10^{-13}$).
123
124 *Prediction of Microbial Short-Chain Fatty Acid Production*
125
126 To evaluate the predicted functional impact of WBF-011 administration, we analyzed the
127 model-predicted production of butyrate and propionate, two key short-chain fatty acids with
128 well-documented metabolic health-promoting, anti-inflammatory, and gut barrier-
129 strengthening properties [27]. Prior work has demonstrated the accuracy of MCMM-based
130 predictions for SCFA production in the human gut microbiome [22], providing a strong rationale
131 for employing this approach to assess the mechanistic contributions of both the probiotic
132 formulation (AMUC, AHAL, BINF, CBEI, and CBUT) and the prebiotic (inulin) used in this study.
133 To systematically dissect the influence of probiotic and prebiotic interventions on SCFA
134 production, we conducted five distinct MCMM simulations on a standard European dietary
135 background: (1) microbiomes from placebo group participants, (2) treatment group
136 microbiomes without any probiotic or prebiotic addition, (3) treatment group microbiomes
137 with probiotic supplementation alone, (4) treatment group microbiomes with prebiotic
138 supplementation alone, and (5) treatment group microbiomes with combined synbiotic
139 supplementation. Following simulation, total MCMM-predicted butyrate and propionate
140 production rates were compared across conditions (Fig. 3).
141 As expected, both the placebo group and the no treatment group exhibited relatively
142 low levels of butyrate production (Fig. 3A, Placebo: 6.59 ± 1.89 mmol/gDW/h; No Treatment:
143 7.53 ± 1.41 mmol/gDW/h). The addition of the WBF-011 probiotic cocktail in the absence of
144 prebiotic supplementation did not significantly alter butyrate production (7.62 ± 1.24
145 mmol/gDW/h), although there was an increasing trend. In contrast, treatment group
146 simulations incorporating inulin, either alone (14.7 ± 1.64 mmol/gDW/h) or in combination with
147 the probiotic cocktail (20.4 ± 1.78 mmol/gDW/h), resulted in significantly elevated butyrate

148 production compared to the first three groups (Mann-Whitney U test, $p < 0.05$). Importantly,
149 butyrate production was also significantly higher in the combined synbiotic condition relative to
150 prebiotic supplementation alone (Mann-Whitney U test, $U = 333.0$, $p = 0.0048$), indicating a
151 synergistic interaction between inulin and the probiotic strains.
152 Similar results were observed for propionate. The placebo, no treatment, and probiotic
153 only group showed low levels of propionate production (Fig. 3B, Placebo: 8.03 ± 0.82
154 mmol/gDW/h; No Treatment: 8.42 ± 0.99 mmol/gDW/h; Probiotic Only: 6.07 ± 0.53
155 mmol/gDW/h). The addition of prebiotic substrate alone or in combination with the probiotic
156 cocktail significantly increased the production of propionate (Prebiotic Only: 63.82 ± 2.72
157 mmol/gDW/h), Prebiotic + Probiotic: 50.67 ± 2.32 mmol/gDW/h, Mann-Whitney U test, $p <$
158 0.05). However, in this case, there was a significant decrease in propionate production in the
159 combined prebiotic-probiotic condition as compared to the prebiotic condition alone (Mann-
160 Whitney U test, $U = 93.0$, $p = 0.0014$). These significant increases in MCMM-predicted butyrate
161 and propionate production rates may help to explain the significant decrease in glucose AUC
162 observed in the WBF-011 treatment group, relative to the placebo [26].
163
164 *C-Reactive Protein Associates with Predicted SCFA Production*
165 In Perraudeau et al. [26], C-reactive protein (CRP), a marker of systemic inflammation, was a
166 primary endpoint measure. In the original study, there were no significant differences in
167 average CRP levels between the treatment and placebo groups. Previous studies have shown
168 that MCMM-based predictions of SCFA production from the gut microbiome show significant
169 associations with the host inflammation state, in line with the known anti-inflammatory effect
170 of these metabolites [22]. We compared the predicted levels of butyrate and propionate
171 production from samples in the treatment group, receiving the combined synbiotic cocktail,
172 against changes in serum CRP levels from baseline to the study endpoint. To determine the
173 overall treatment effect, change in CRP from Week 0 to Week 12 (ΔCRP) was compared against
174 the change in butyrate or propionate production from pre-treatment to post-treatment
175 (Δbutyrate and Δpropionate, respectively).
176 Δpropionate showed a significant negative association with ΔCRP within the treatment
177 group (Fig. 4A, linear regression, $r = -0.48$, $p = 0.025$). However, the association between
178 Δbutyrate and ΔCRP did not reach significance (Fig. 4B, linear regression, $r = 0.22$, $p = 0.33$).
179
180 *Personalized MCMM-Predicted Engraftment and SCFA Production Predictions for a Probiotic*
181 *Cocktail Across Different Prebiotic and Dietary Backgrounds in a Large Observational Cohort*
182 We ran MCMM simulations in a cohort of 156 individuals from a former precision wellness
183 company (Arivale) with newly-generated stool metagenomic sequencing data, balanced for age
184 and sex. To demonstrate the broader applicability of this methodology in designing
185 personalized synbiotics, growth of WBF-011 strains was simulated across six prebiotic and

186 dietary contexts: (1) a standard European diet without prebiotic supplementation, (2) a
187 standard European diet supplemented with inulin, (3) a standard European diet supplemented
188 with pectin, (4) a standard European diet supplemented with resistant starch, (5) a standard
189 European diet supplemented with maltodextrin, (6) a standard European diet supplemented
190 with hemp seed, (7) a standard European diet supplemented with psyllium husk, and (8) a
191 standard high-fiber diet.

192 Probiotic engraftment predictions varied across prebiotic and dietary backgrounds (Fig.
193 5A). For instance, the switch from a standard European diet to a high-fiber diet resulted in a
194 much higher average engraftment rate for AMUC (growth in 100% of samples, versus 57% on
195 the standard European diet), but a decrease in engraftment for BINF (growth in 17% of samples,
196 versus 42% on the standard European diet). MCMM-predicted butyrate and propionate
197 production rates increased significantly as a result of both prebiotic and probiotic addition (Fig.
198 5B-C). The addition of probiotic consortia showed significant increases in predicted butyrate
199 production in every case, except for when no prebiotic substrate was added (Mann-Whitney U
200 test, $p < 0.05$). For propionate, a significant decrease in predicted production was observed in
201 every case (Mann-Whitney U test, $p < 0.05$). A shift away from a standard European diet to a
202 high-fiber diet showed the largest increase in both predicted butyrate and propionate
203 production rates (Fig. 5B-C, Butyrate: Mann-Whitney U test, $U = 251$, $p = 1.4x10^{-50,}$; Propionate:
204 Mann-Whitney U test, $U = 4.0$, $p = 1.3x10^{-52,}$).

205 For each individual, the optimal prebiotic-probiotic combination on the standard
206 European diet was identified, in terms of maximizing predicted butyrate or propionate
207 production rates. While some patterns emerged, the optimal intervention varied across
208 individuals (Figs. S1-2). For butyrate production, the most common optimal treatment was the
209 use of starch in combination with the 5-strain probiotic cocktail. For propionate production,
210 psyllium husk with no probiotic cocktail was the most common optimal intervention. Overall, a
211 personalized optimal solution resulted in significantly higher predicted levels of propionate and
212 butyrate production when compared with the 'standard of care' synbiotic treatment, which was
213 defined as combining inulin with the probiotic cocktail, as in the original WB-011 trial (Fig. 6).

214 **Discussion**

215 The ability of an orally administered probiotic to successfully engraft in the gut is influenced by
216 multiple ecological and host-specific factors, including the pre-existing composition of the gut
217 microbiome and the background diet. A method for the rational prediction of probiotic
218 engraftment and health-relevant microbial metabolite production, in the context of a given
219 microbiota and diet, would open up new avenues for precision synbiotic design. Prior work by
220 our group has demonstrated that our microbial community-scale metabolic modeling (MCMM)
221 platform can be leveraged to predict personalized SCFA production rates and personalized
222 pathobiont engraftment risk [22,23]. In order to validate our MCMM methodology in the context

223 of synbiotic design, we leverage qPCR data from the WBF-011 synbiotic trial to determine
224 whether or not we can accurately predict relevant outcomes. The WBF-011 trial showed
225 variable engraftment rates across the five tested probiotic organisms: *Akkermansia muciniphila*
226 (AMUC), *Bifidobacterium infantis* (BINF), *Clostridium beijerinckii* (CBEI), *Anaerobutyricum hallii*
227 (AHAL), and *Clostridium butyricum* (CBUT). AMUC and BINF showed engraftment across most of
228 the participants, while CBEI, AHAL, and CBUT rarely engrafted. Given this heterogeneity, these
229 trial data represented an ideal validation-case for our MCMM predictions.
230 Despite the inherent complexity of predicting probiotic growth, the MCMM-based
231 predictive framework demonstrated substantial accuracy, showing over 85% agreement with
232 observed probiotic engraftment patterns (Fig. 2A). These models incorporate key ecological
233 determinants, like endogenous microbiome composition and the availability of prebiotic and
234 dietary substrates, to estimate probiotic growth rates, which are closely aligned with
235 experimental qPCR data. Notably, of the 105 total comparisons, 90 were accurately predicted,
236 with 57 instances correctly classified as non-growth and 33 correctly classified as growth (Fig.
237 2B). This high level of accuracy in engraftment prediction was achieved in spite of the fact that
238 we lacked personalized constraints on dietary intake (i.e., a standard European diet was applied
239 to each model).
240 A fundamental goal of probiotic and prebiotic supplementation is to modulate the
241 production of key microbial metabolites that support host health. Among these, short-chain
242 fatty acids (SCFAs)—such as butyrate and propionate—are particularly significant due to their
243 roles in maintaining gut barrier integrity, regulating proper immune function, and supporting
244 metabolic homeostasis [22,27]. Synbiotic administration provides a means of enhancing SCFA
245 production, and MCMMs can be leveraged to predict these metabolic shifts. As anticipated,
246 MCMMs predicted a significant increase in the total production of butyrate and propionate in
247 response to inulin supplementation, consistent with its role as a fermentable dietary fiber that
248 serves as an ideal substrate for SCFA biosynthesis (Fig. 3). Notably, our analysis also revealed a
249 synergistic effect between prebiotic administration and the WBF-011 probiotic cocktail. While
250 inulin alone significantly increased butyrate production compared to baseline, the combination
251 of inulin with WBF-011 led to an even greater increase (Fig. 3A). This finding aligns with prior
252 studies highlighting the contributions of both *Bifidobacterium longum* and *Akkermansia*
253 *muciniphila*, key members of the WBF-011 consortium, to butyrate production through cross-
254 feeding interactions within the gut microbiota [28–30]. In contrast, both inulin alone and the
255 prebiotic-probiotic combination increased propionate levels relative to the baseline, but the
256 synbiotic combination resulted in significantly lower propionate production compared to the
257 prebiotic alone (Fig. 3B). These results suggest that this probiotic cocktail may bias SCFA
258 production away from propionate towards butyrate, shifting the metabolic output of a
259 community. Such metabolic trade-offs are well-documented in microbial ecosystems, where
260 competition for substrates influences the balance of SCFA production [21,22,27,31].

261 Next, we sought to identify associations between synbiotic-induced changes in
262 predicted SCFA production and the primary outcome variables. Perraudeau et al. identified a
263 significant drop in the area under the curve (AUC) for postprandial glucose levels during a
264 standardized meal-tolerance test over the 12-week trial period in the treatment group, but not
265 in the placebo group [26]. This drop in glucose AUC mirrors the significant increase we found in
266 MCMM-predicted butyrate and propionate production rates in response to the symbiotic
267 treatment (Fig. 3). Given that increased intestinal SCFA availability has been linked to improved
268 glycemic control [32], the observed metabolic effects in this study may be partially attributable to
269 the enhanced SCFA production induced by the WBF-011 and inulin combination [33]. Future
270 intervention studies could further refine these insights by integrating longitudinal metabolomic
271 and host-response data to establish more direct mechanistic links between microbial SCFA
272 production and host metabolic outcomes.
273 CRP was the primary immunological endpoint measured during the WBF-011 trial, as it
274 is a well established metric of systemic inflammation [34]. Based on collected patient data, no
275 significant difference was observed in endpoint CRP measures between the treatment and
276 placebo arms of the study. However, we observed that within the treatment arm, there was a
277 significant negative association between the change in CRP and the model-predicted change in
278 propionate production from Week 0 to Week 12 (Fig 4A). This relationship was not observed for
279 butyrate. While butyrate is generally thought to be a more potent anti-inflammatory SCFA,
280 propionate can also reduce inflammation [35] and prior work from our group has observed a
281 significant negative relationship between diet-mediated inflammation and MCMM-predicted
282 propionate production [22].
283 Given the strong engraftment validation we observed in the WBF-011 trial, we decided
284 to expand our MCMM simulations to a larger cohort where we could explore engraftment and
285 SCFA production predictions across a wider range of probiotics, prebiotics, and dietary
286 backgrounds. Simulation results from a cohort of 156 generally-healthy individuals showed that
287 variation in prebiotic and dietary inputs could substantially alter engraftment outcomes across
288 individuals. We observed that a switch from the standard European diet to a high-fiber diet
289 greatly improved the engraftment success of *Akkermansia muciniphila*, a probiotic shown to
290 improve post-prandial glucose responses [26]. Additionally, microbial production of butyrate and
291 propionate increased with prebiotic supplementation and with a switch to a standard high fiber
292 diet. Not all individuals responded to the same prebiotic fibers, and there was a heterogenous
293 response in terms of the most optimal treatment for each individual, indicating how MCMMs
294 could be a valuable tool for optimizing prebiotic and probiotic pairings. Ultimately, this
295 methodology could be leveraged to improve the administration of probiotics and prebiotics,
296 depending on the baseline gut microbiome composition and the dietary background of the
297 host.

298 During the course of our work on this project, we found that the single-strain species-
299 level AGORA1 GEM for *Akkermansia muciniphila* failed to predict growth in any sample
300 following its introduction, whereas the multi-strain species-level AGORA2 GEM successfully
301 predicted growth consistent with experimental results. For most other commensal species in
302 our simulations, we had multiple AGORA1 representative strains that could be included in a
303 pan-strain model [36]. We hypothesize that the improvement in *Akkermansia* engraftment
304 predictions between AGORA1 and AGORA2 stems from the inclusion of four *A. muciniphila*
305 strains in AGORA2, compared to only a single strain in AGORA1. Given that individual strain-
306 level models are often imperfectly curated, greater strain-level representation in species-level
307 GEMS likely captures a broader range of metabolic capabilities, which appears to lead to better
308 agreement between model predictions and experimental outcomes. While constructing GEMs
309 for all possible strains remains impractical, increasing strain diversity within species-level
310 models appears to offer clear benefits in these community-scale simulations. Interestingly, this
311 phenomenon may be rooted in the biology of real-world ecosystems, where we often observe
312 the coexistence of 2-3 strains for each bacterial species in the human gut [37].
313 Despite promising results, there are certain limitations implicit to the methodology
314 presented here. Principal among these is that existing GEM databases do not include all extant
315 strains for a given gut bacterial species. The consequence of this is that MCMM-based analyses
316 such as these are limited to species-level resolution, using models that summarize the
317 metabolic capacity of available strains within a given species. For a trial such as this, strain-
318 specific engraftment cannot be isolated from growth predictions of endogenous strains. For this
319 reason, we centered our engraftment definition on enrichment of a species above its baseline
320 level following treatment. Future work should focus on accounting for strain-level differences in
321 metabolic capacity that differ between probiotic and endogenous strains of a given species.
322 Another limitation of this analysis was the lack of participant dietary intake data. Better
323 constraints on personalized dietary intake should further improve the predictive accuracy that
324 we observed in the current analysis, which assumed that everyone was eating the standard
325 European diet. Finally, the current methodology for constructing and solving MCMMs does not
326 account for spatial structure or host physiology within the gut. For instance, *Akkermansia*
327 *muciniphila* typically grows within the mucus layer of the colonic epithelium, in a different
328 microenvironment than many other taxa within the microbiota. For this reason, it is more
329 closely tied to the colonic epithelium, and the production of host-derived compounds. Future
330 work should aim to integrate MCMMs with metabolic models of the colonic epithelium [38],
331 which may help to further improve predictions.
332 Taken together, these findings demonstrate the utility of MCMMs as a predictive
333 framework for assessing synbiotic interventions at the individual and population levels. By
334 integrating metabolic modeling with experimental validation, we highlight key ecological and
335 metabolic determinants of probiotic engraftment success and SCFA production, providing a

pathway for more targeted microbiome-based therapies. However, realizing the full potential of these models will require continued refinement, including improved strain-level resolution, more comprehensive dietary intake data, and enhanced host-microbiome interaction modeling. Future research should aim to bridge these gaps by incorporating multi-omics approaches, longitudinal sampling, and personalized dietary profiling. Ultimately, leveraging MCMMs in a clinical setting could enable precision microbiome therapeutics tailored to an individual's metabolic and inflammatory profile, optimizing probiotic and prebiotic efficacy across diverse patient populations.

Methods

Data collection

Validation data used in this study were obtained from Perraudeau et al. (2020). The study cohort consisted of 76 participants previously diagnosed with type 2 diabetes. Participants were randomized into two experimental groups (N = 27 and N = 23) and a placebo group (N = 26). 10, 6 and 2 participants were lost to follow-up in each study arm, respectively. Those in the experimental groups received one of two probiotic formulations, WBF-010 or WBF-011. WBF-010 contained strains of *Bifidobacterium longum subsp. infantis*, *Clostridium butyricum*, and *Clostridium beijerinckii*. WBF-011 included the same strains as WBF-010 with the addition of *Akkermansia muciniphila* and *Anaerobutyricum hallii*. Both probiotic formulations were supplemented with a small amount of inulin (0.3 grams), a prebiotic derived from chicory root. Participants in all three study arms followed the intervention for 12 weeks, consuming three capsules twice daily. The primary metabolic endpoint assessed in the original trial was the change in the area under the curve (AUC) for glucose during a standard three-hour meal-tolerance test (MTT) conducted at baseline and after 12 weeks. The ΔAUC values were calculated by subtracting baseline AUC from the 12-week AUC. Analysis revealed that WBF-011, but not WBF-010, led to a significant shift in ΔAUC compared to the placebo, so only the WBF-011 study arm was used for downstream microbial community-scale metabolic model (MCMM) predictions.

Additional data used in the analysis were collected from Arivale, Inc. (Seattle, WA). Arivale closed its operations in 2019. De-identified metagenomic data from patient-collected fecal samples was collected and used to construct MCMMs as described below. Participants included in the analysis (N = 156) were adults in the United States (92 female, 64 male sex assigned at birth), with average age 47.4 ± 1.0 years. Metagenomes are available on the NCBI Sequence Read Archive under accession number PRJNA1262070.

Model Construction

Metagenomic sequencing was performed on stool samples collected at baseline and after 12 weeks. Raw sequencing reads were processed using Kraken2 (v1.01) for taxonomic

classification, and Bracken was used to refine taxonomic abundance estimates [39,40]. Read counts were normalized to relative abundance before their incorporation into downstream modeling workflows. MCMMs were constrained using metagenomic relative abundance profiles for all baseline samples using MICOM (v0.37.0), a framework for simulating microbial community metabolism [21]. Taxonomic profiles from baseline samples were mapped to genome-scale metabolic models (GEMs) from the AGORA database (v1.03) [36]. A relative abundance threshold of 0.001 was applied to exclude taxa representing less than 0.1% of the community composition.

For experimental group samples, probiotic supplementation was simulated *in silico* by modifying the baseline taxonomic composition. The relative abundances of pre-existing taxa were proportionally reduced to 95% of their original values, while five probiotic species from WBF-011 were introduced at a total relative abundance of 5% (1% each). The 5% supplementation level was selected to provide a detectable perturbation to the community while maintaining ecological realism.

For *Akkermansia muciniphila* (AMUC), we used an updated species-level metabolic model from the AGORA2 database, as the AGORA1 version failed to predict growth under any simulated conditions.

Model Growth

Community growth simulations were performed using MICOM's cooperative tradeoff optimization, which balances individual taxon growth with overall community-wide metabolic efficiency. A tradeoff parameter of 0.99 was applied to ensure a balance between individual taxon viability and community-level metabolic fluxes. All models were supplied with a simulated growth medium reflective of an average European diet. In the absence of detailed dietary recall data, this can be used to approximate the average dietary consumption of individuals in North America, where this study took place. In the WBF-011 trial, inulin was included as an additional substrate in the medium to account for the prebiotic component of the synbiotic intervention. For expanded analysis in Arivale, inulin, pectin, starch, maltodextrin, cellulose (hemp seed), or arabinoxylan (psyllium husk), were added to the standard European diet to test prebiotic additions. Simulation using a high-fiber diet was also done. All dietary combinations were used to predict model outputs. Predicted growth rates for the five probiotic species were extracted from MICOM model outputs. To facilitate direct comparison with qPCR data in the WBF-011 trial, predicted growth rates were binarized using a threshold of 10^{-3} h^{-1}. Growth rates below this value were classified as non-engraftment (0), while those above were classified as successful engraftment (1).

qPCR Comparison

qPCR data collected from the original study was used as ground truth for the validation of model-based predictions. qPCR results failing quality control and filtering were removed. Inverse cycle threshold (1/Ct) was used as a proxy for species abundance. For each probiotic species, a low end threshold was defined by the mean value for 1/Ct for that species at Week 0. 1/Ct values from Week 12 were binarized around this threshold, for comparison with binarized MCMM-predicted growth rates.

Statistical analysis

All statistical analysis conducted in this study was computed using Scipy (v 1.13.1) [41]

To assess the concordance between binarized MICOM-predicted engraftment and qPCR observations, the Cohen's Kappa statistic was computed. This measure quantifies the level of agreement beyond what would be expected by chance, providing insight into the predictive accuracy of MCMMs for probiotic engraftment outcomes. Furthermore, Fisher's exact test was used to evaluate whether the observed agreement between MICOM predictions and qPCR results in the confusion matrix was statistically significant.

Significance in differences in predicted butyrate and propionate between treatment groups in both the probiotic trial and the Arivale cohort (Fig. 3, Fig. 5) was computed using non-parametric Mann-Whitney U test. Significance in differences between predicted butyrate and propionate between optimal and standard of care interventions in the Arivale cohort (Fig. 6) was also determined using non-parametric Mann-Whitney U test.

Association between measured CRP values and predicted SCFA production was conducted using ordinary least squares linear regression. In the absence of available metadata, no confounding variables were used.

Data and Code Availability

qPCR and metagenomic sequencing data for the trial by Perraudeau et al. 2020 are available upon request. Metagenomic sequencing data for the 156 members of the Arivale dataset are available on the NCBI Sequence Read Archive under accession number PRJNA1262070. All analysis conducted in the manuscript can be found at https://github.com/Gibbons-Lab/2024_probiotic_engraftment.

Competing Interests Statement

This work was funded, in part, by a research grant from Pendulum (to SMG), which is the company that manufactured the synbiotic tested in Perraudeau et al. (2020). Pendulum had no part in the design or conduct of this study or the writing of this manuscript. SMG is a paid member of the scientific advisory board for Thorne. This work is unrelated to Thorne, and Thorne had no involvement in the design or conduct of this study or in the writing of the manuscript.

Acknowledgements

This work was supported by research funding from Pendulum Therapeutics, Inc., by the National Institute of Diabetes and Digestive and Kidney Diseases (NIDDK) of the National Institutes of Health (NIH) under award number R01DK133468, and by a Global Grants for Gut Health Award from Nature Portfolio and Yakult (to S.M.G.). Thanks to Alex Carr for helpful discussions on MCMM engraftment assessment.

References

1. Gul, S. & Durante-Mangoni, E. Unraveling the puzzle: Health benefits of probiotics-A comprehensive review. *J. Clin. Med.* **13**, 1436 (2024).
2. Latif, A. *et al.* Probiotics: mechanism of action, health benefits and their application in food industries. *Front. Microbiol.* **14**, 1216674 (2023).
3. Ansari, F. *et al.* The role of probiotics and prebiotics in modulating of the gut-brain axis. *Front. Nutr.* **10**, 1173660 (2023).
4. Oliphant, K. & Allen-Vercoe, E. Macronutrient metabolism by the human gut microbiome: major fermentation by-products and their impact on host health. *Microbiome* **7**, 91 (2019).
5. Rackerby, B., Van De Grift, D., Kim, J. H. & Park, S. H. Effects of Diet on Human Gut Microbiome and Subsequent Influence on Host Physiology and Metabolism. *Gut Microbiome and Its Impact on Health and Diseases* 63–84 Preprint at https://doi.org/10.1007/978-3-030-47384-6_3 (2020).
6. Belkaid, Y. & Hand, T. W. Role of the microbiota in immunity and inflammation. *Cell* **157**, 121–141 (2014).
7. Zheng, D., Liwinski, T. & Elinav, E. Interaction between microbiota and immunity in health and disease. *Cell Res.* **30**, 492–506 (2020).
8. Ryan, F. J. *et al.* Bifidobacteria support optimal infant vaccine responses. *Nature* (2025) doi:10.1038/s41586-025-08796-4.
9. Nagpal, R. *et al.* Human-origin probiotic cocktail increases short-chain fatty acid production via modulation of mice and human gut microbiome. *Sci. Rep.* **8**, 12649 (2018).
10. Markowiak-Kopeć, P. & Śliżewska, K. The effect of probiotics on the production of short-chain fatty acids by human intestinal microbiome. *Nutrients* **12**, 1107 (2020).
11. Snigdha, S. *et al.* Probiotics: Potential novel therapeutics for microbiota-gut-brain axis dysfunction across gender and lifespan. *Pharmacology & Therapeutics* **231**, 107978 (2022).

12. Mazziotta, C., Tognon, M., Martini, F., Torreggiani, E. & Rotondo, J. C. Probiotics mechanism of action on immune cells and beneficial effects on human health. *Cells* **12**, 184 (2023).
13. Cristofori, F. *et al.* Anti-inflammatory and immunomodulatory effects of probiotics in gut inflammation: A door to the body. *Front. Immunol.* **12**, 578386 (2021).
14. Maldonado-Gómez, M. X. *et al.* Stable engraftment of Bifidobacterium longum AH1206 in the human gut depends on individualized features of the resident microbiome. *Cell Host Microbe* **20**, 515–526 (2016).
15. Dsouza, M. *et al.* Colonization of the live biotherapeutic product VE303 and modulation of the microbiota and metabolites in healthy volunteers. *Cell Host Microbe* **30**, 583–598.e8 (2022).
16. Coyte, K. Z. & Rakoff-Nahoum, S. Understanding Competition and Cooperation within the Mammalian Gut Microbiome. *Curr Biol* **29**, R538–R544 (2019).
17. Spencer, S. P., Fragiadakis, G. K. & Sonnenburg, J. L. Pursuing Human-Relevant Gut Microbiota-Immune Interactions. *Immunity* **51**, 225–239 (2019).
18. Fujita, H. *et al.* Alternative stable states, nonlinear behavior, and predictability of microbiome dynamics. *Microbiome* **11**, 63 (2023).
19. Orth, J. D., Thiele, I. & Palsson, B. Ø. What is flux balance analysis? *Nat. Biotechnol.* **28**, 245–248 (2010).
20. Diener, C. & Gibbons, S. M. More is Different: Metabolic Modeling of Diverse Microbial Communities. *mSystems* **8**, e0127022 (2023).
21. Diener, C., Gibbons, S. M. & Resendis-Antonio, O. MICOM: Metagenome-Scale Modeling To Infer Metabolic Interactions in the Gut Microbiota. *mSystems* **5**, (2020).
22. Quinn-Bohmann, N. *et al.* Microbial community-scale metabolic modelling predicts personalized short-chain fatty acid production profiles in the human gut. *Nature Microbiology* 1–13 (2024).

23. Carr, A., Baliga, N. S., Diener, C. & Gibbons, S. M. Personalized Clostridioides difficile engraftment risk prediction and probiotic therapy assessment in the human gut. *bioRxiv* (2024) doi:10.1101/2023.04.28.538771.

24. Orellana, E. *et al.* Sustainable Food Waste Management in Anaerobic Digesters: Prediction of the Organic Load Impact by Metagenome-Scale Metabolic Modeling. *Environ Sci Technol* (2025) doi:10.1021/acs.est.4c11180.

25. Marcelino, V. R. *et al.* Disease-specific loss of microbial cross-feeding interactions in the human gut. *Nat Commun* **14**, 6546 (2023).

26. Perraudeau, F. *et al.* Improvements to postprandial glucose control in subjects with type 2 diabetes: a multicenter, double blind, randomized placebo-controlled trial of a novel probiotic formulation. *BMJ Open Diabetes Res. Care* **8**, e001319 (2020).

27. Tan, J. *et al.* The role of short-chain fatty acids in health and disease. *Adv Immunol* **121**, 91–119 (2014).

28. Rivière, A., Selak, M., Lantin, D., Leroy, F. & De Vuyst, L. Bifidobacteria and butyrate-producing colon bacteria: Importance and strategies for their stimulation in the human gut. *Front. Microbiol.* **7**, 979 (2016).

29. Falony, G., Vlachou, A., Verbrugghe, K. & De Vuyst, L. Cross-feeding between Bifidobacterium longum BB536 and acetate-converting, butyrate-producing colon bacteria during growth on oligofructose. *Appl. Environ. Microbiol.* **72**, 7835–7841 (2006).

30. Chia, L. W. *et al.* Deciphering the trophic interaction between Akkermansia muciniphila and the butyrogenic gut commensal Anaerostipes caccae using a metatranscriptomic approach. *Antonie Van Leeuwenhoek* **111**, 859–873 (2018).

31. Tuncil, Y. E., Thakkar, R. D., Marcia, A. D. R., Hamaker, B. R. & Lindemann, S. R. Divergent short-chain fatty acid production and succession of colonic microbiota arise in fermentation of variously-sized wheat bran fractions. *Sci Rep* **8**, 16655 (2018).

32. Corbin, K. D. *et al.* Host-diet-gut microbiome interactions influence human energy balance:

a randomized clinical trial. *Nat Commun* **14**, 3161 (2023).

33. Wijdeveld, M. *et al.* Intestinal acetate and butyrate availability is associated with glucose metabolism in healthy individuals. *iScience* **26**, 108478 (2023).
34. Nehring, S. M., Goyal, A. & Patel, B. C. *C Reactive Protein*. (StatPearls Publishing, 2023).
35. Filippone, A. *et al.* The Anti-Inflammatory and Antioxidant Effects of Sodium Propionate. *Int J Mol Sci* **21**, (2020).
36. Magnúsdóttir, S. *et al.* Generation of genome-scale metabolic reconstructions for 773 members of the human gut microbiota. *Nat. Biotechnol.* **35**, 81–89 (2017).
37. Wolff, R., Shoemaker, W. & Garud, N. Ecological Stability Emerges at the Level of Strains in the Human Gut Microbiome. *mBio* **14**, e0250222 (2023).
38. Jiang, B. *et al.* Understanding disease-associated metabolic changes in human colon epithelial cells using ColonEpithelium metabolic reconstruction. *bioRxiv* (2024) doi:10.1101/2024.10.22.619644.
39. Wood, D. E., Lu, J. & Langmead, B. Improved metagenomic analysis with Kraken 2. *Genome Biol.* **20**, 257 (2019).
40. Lu, J., Breitwieser, F. P., Thielen, P. & Salzberg, S. L. Bracken: estimating species abundance in metagenomics data. *PeerJ Comput. Sci.* **3**, e104 (2017).
41. Virtanen, P. *et al.* SciPy 1.0: fundamental algorithms for scientific computing in Python. *Nat. Methods* **17**, 261–272 (2020).

Figures and Captions

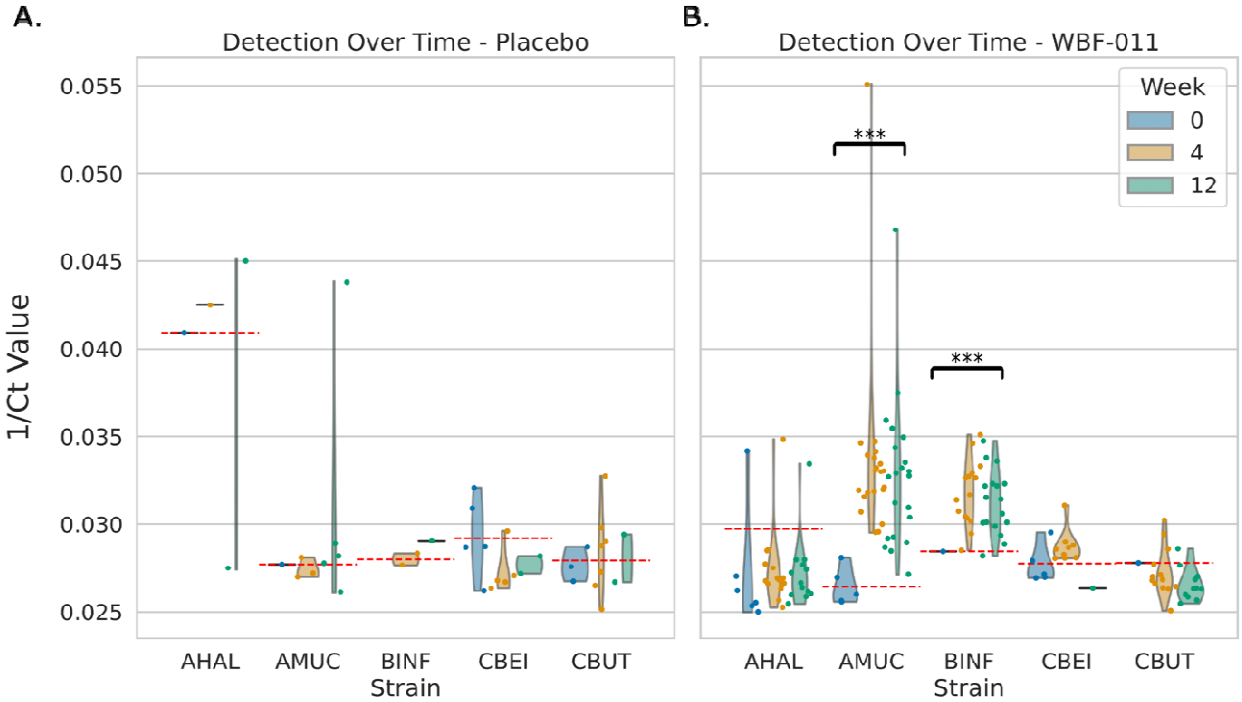

Figure 1. qPCR quantification of probiotic strain abundances in WBF-011 and placebo arms. (A) There were no significant enrichments in probiotic strains over time in the placebo treatment group, although a few samples showed high 1/Ct values (likely due to primer binding to phylogenetically related endogenous strains). (B) There was a significant enrichment in AMUC and BINF probiotics in the WBF-011 treatment arm. There was no enrichment of CBEI, CBUT and AHAL probiotics in the WBF-011 treatment arm. Significant increase determined by Mann-Whitney U test, *** = $p < 0.001$.

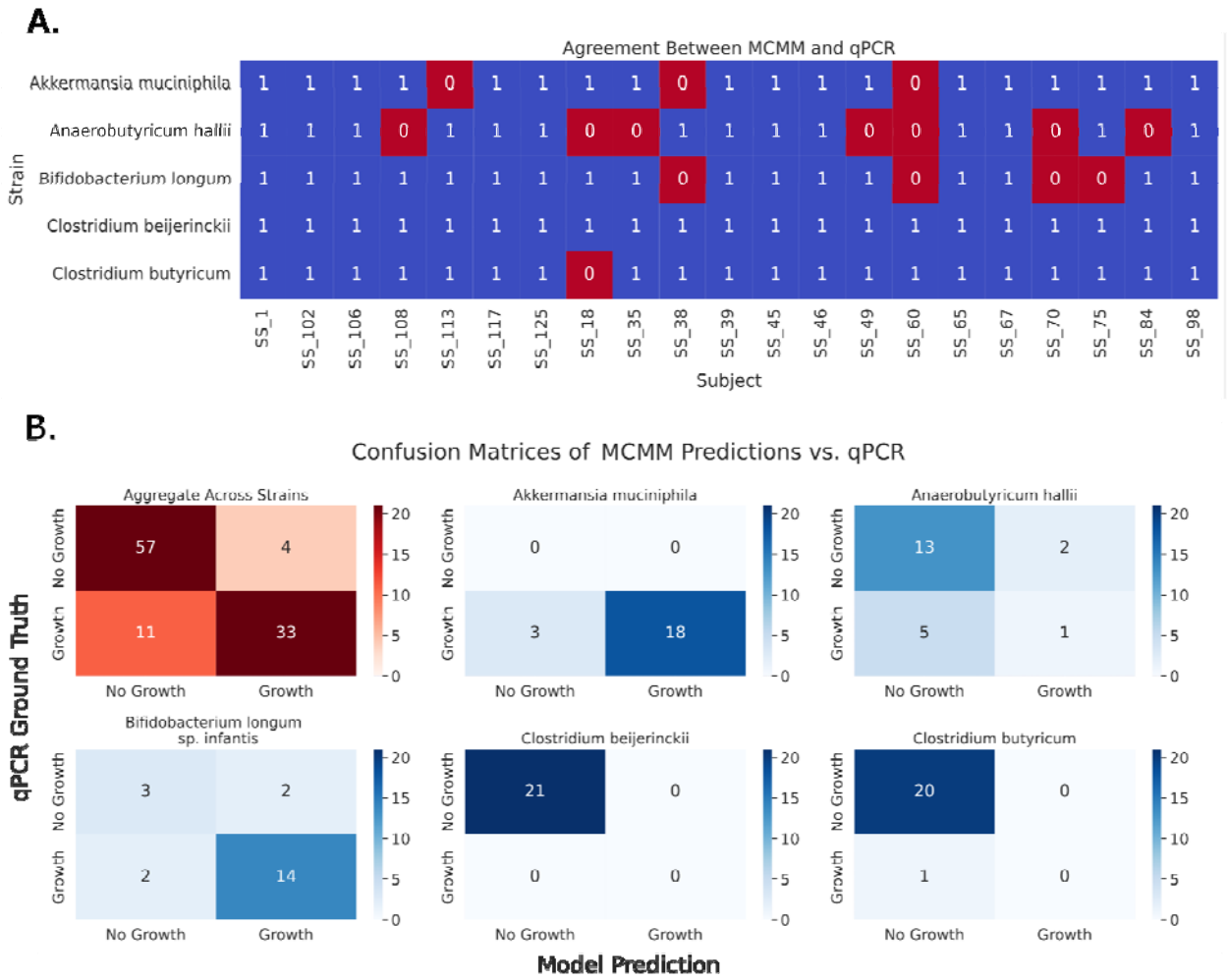

Figure 2. MCMM predictions for probiotic growth show significant agreement with qPCR engraftment thresholds. (A) MCMM-predicted growth rates binarized around a threshold of 0.001 agree with qPCR detection thresholds in 90 out of 105 observations (Cohen's κ = 0.70, indicating substantial agreement). Blue boxes containing a "1" indicate agreement, red boxes containing a "0" indicate disagreement between the model and the qPCR data. (B) Confusion matrices describing results across and within probiotic strains, showing highly significant agreement (Fisher's Exact Test, aggregate results across all strains, $p = 1.3 \times 10^{-13}$).

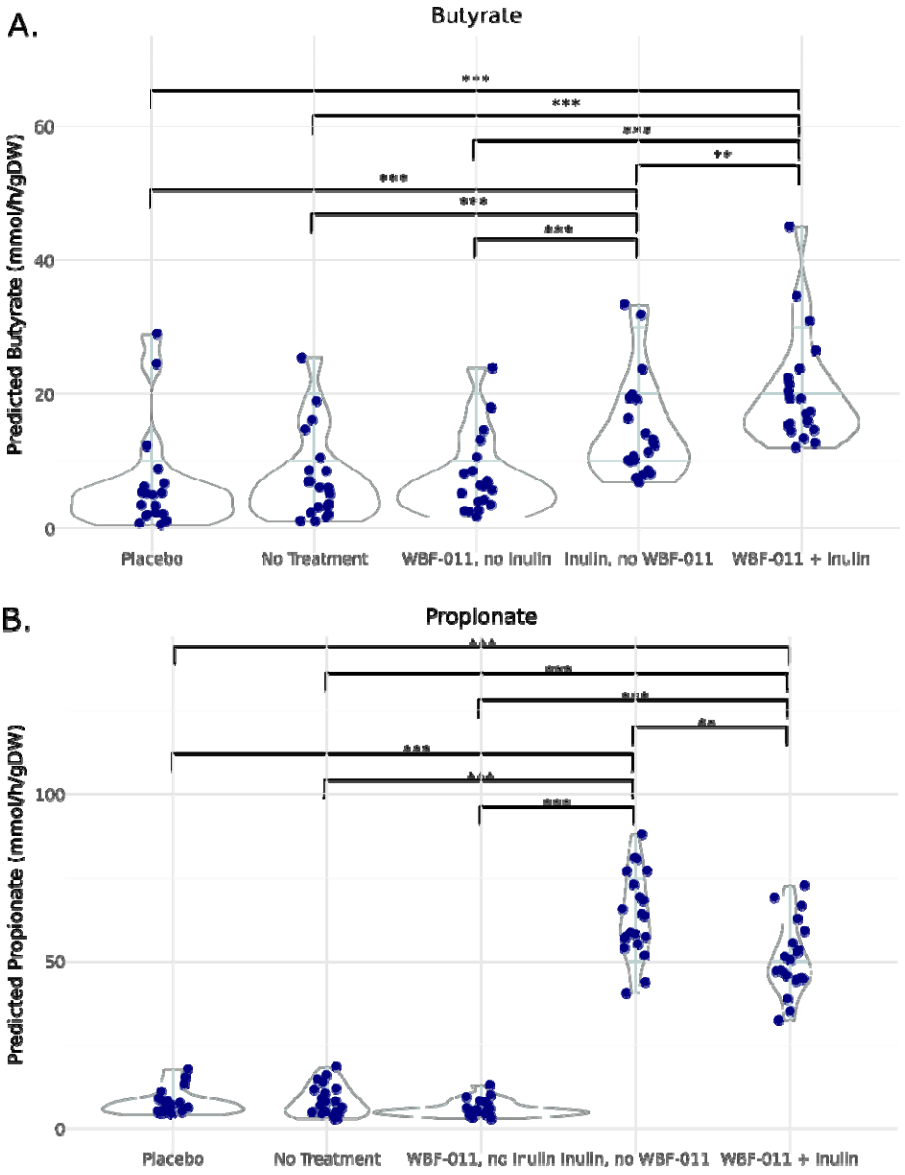

Figure 3. MCMM–predicted SCFA production rates shift in response to prebiotic and probiotic treatment. (A) Butyrate production in MCMM simulations increased in response to prebiotic and synbiotic supplementation. Significant increases were observed with inulin alone, as well as with the combined inulin-WBF-011 treatment. (B) Propionate production in MCMM simulations also increased with inulin and synbiotic treatment, relative to no treatment. However, propionate production declined in the synbiotic condition, relative to the prebiotic-only condition. Each point represents the predicted production level for a single sample. **: $p < 0.01$, ***: $p < 0.001$, Mann-Whitney U test.

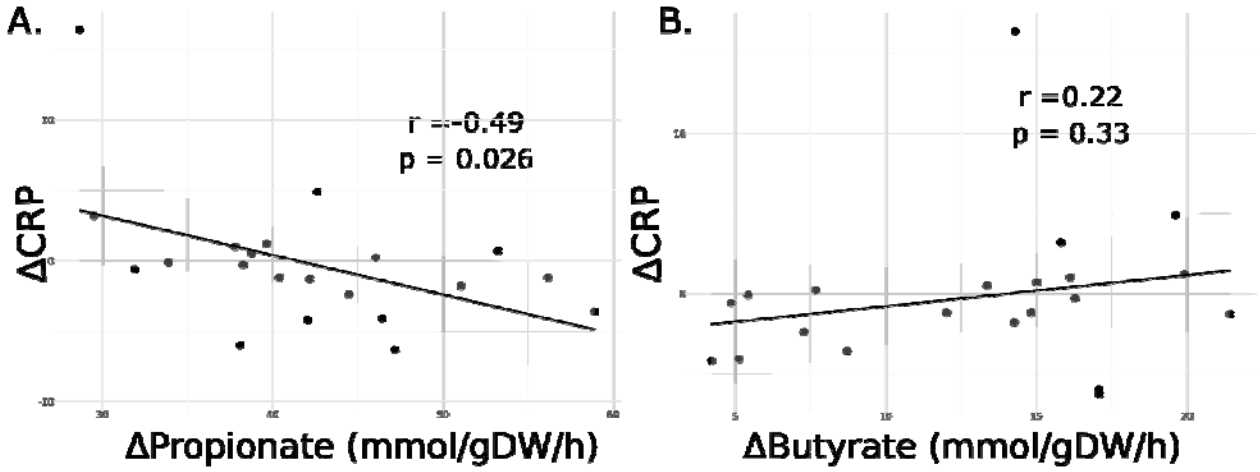

Figure 4. Post-intervention changes in inflammatory marker CRP shows association with MCMM-predicted changes in propionate, but not butyrate, production rates relative to baseline in the synbiotic treatment group. (A) ΔCRP showed significant negative association with MCMM-predicted Δpropionate in models treated with the synbiotic (linear regression, r = -0.49, p = 0.026, t-test for slope). (B) MCMM-predicted Δbutyrate did not show a significant association with ΔCRP (linear regression, r = 0.22, p = 0.33, t-test for slope).

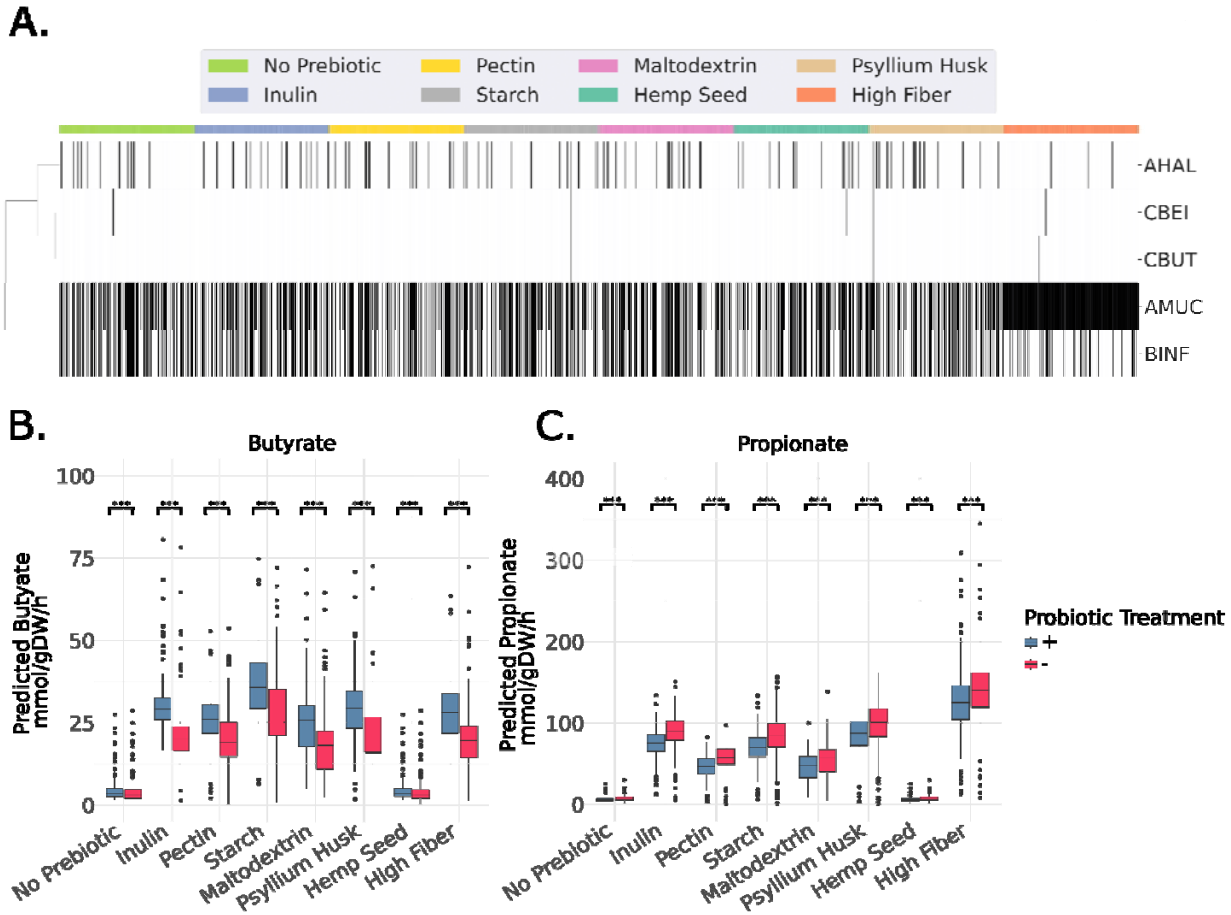

Figure 5. MCMM-predicted engraftment and SCFA production rates across simulated probiotic and prebiotic interventions in a cohort of generally-healthy Americans. (A) Using a cohort of 156 individuals, we predicted engraftment, using a growth rate binarization threshold of 10^{-3}. Differential engraftment was observed across prebiotic and dietary backgrounds. Black cells denote engraftment, while white cells indicate non-engraftment. (B-C) Butyrate and propionate production rates were increased upon treatment with prebiotic substrates on a standard European diet (inulin, pectin, resistant starch, maltodextrin, psyllium or hemp seed), or with a shift from a standard European to a standard high-fiber diet. Probiotics tended to increase butyrate production rates and decrease propionate production rates, relative to the prebiotic-alone treatments. Color encoding demonstrates the effect of adding a probiotic cocktail to the prebiotic/dietary treatments. Significance determined by Mann-Whitney U-test, *** = $p<0.001$.

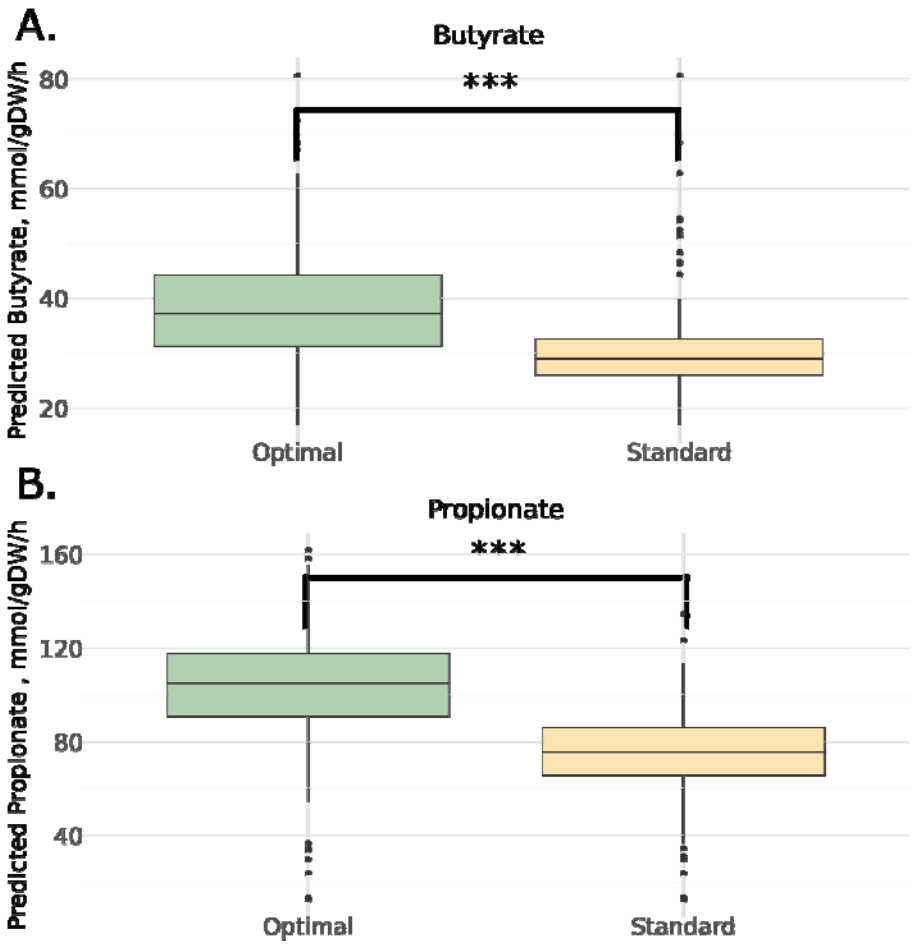

Figure 6. Personalized treatments outperform standard of care. For both SCFAs, an optimal prebiotic and/or probiotic treatment combination was selected and compared against a standard treatment, which consisted of inulin and the 5-strain probiotic cocktail. In both cases, the individual-specific optimal treatment showed significantly higher levels of production. Significance determined by Mann-Whitney U-test, *** = $p<0.001$.

Supplementary Figure Captions

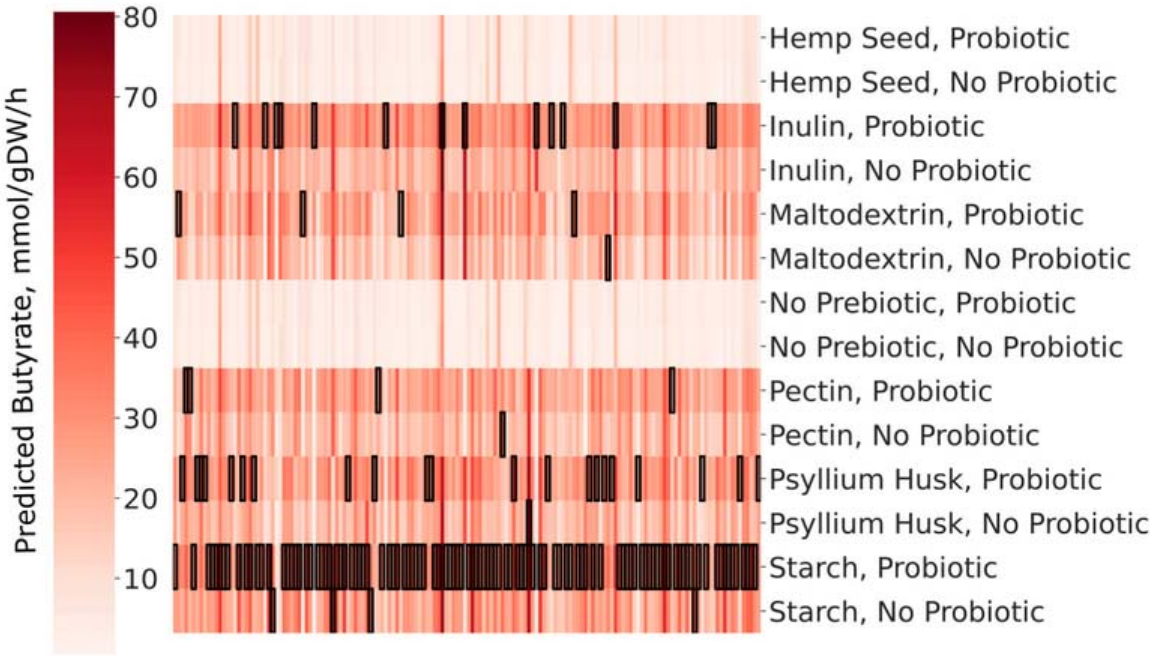

Figure S1. Individual-specific optimal synbiotic treatments for maximizing butyrate production. MCMM-predicted butyrate production varied substantially across individuals (N = 156) in response to different synbiotic combinations. The combination of starch and the five-strain probiotic cocktail produced the highest butyrate flux in the greatest number of individuals. However, every other prebiotic/probiotic combination was optimal for at least one individual, with the exceptions of: (1) hemp seed, (2) the no-probiotic condition, and (3) inulin with no probiotic cocktail. Heatmap colors indicate predicted butyrate flux (mmol/gDW/h), and black boxes denote the most effective treatment for each sample.

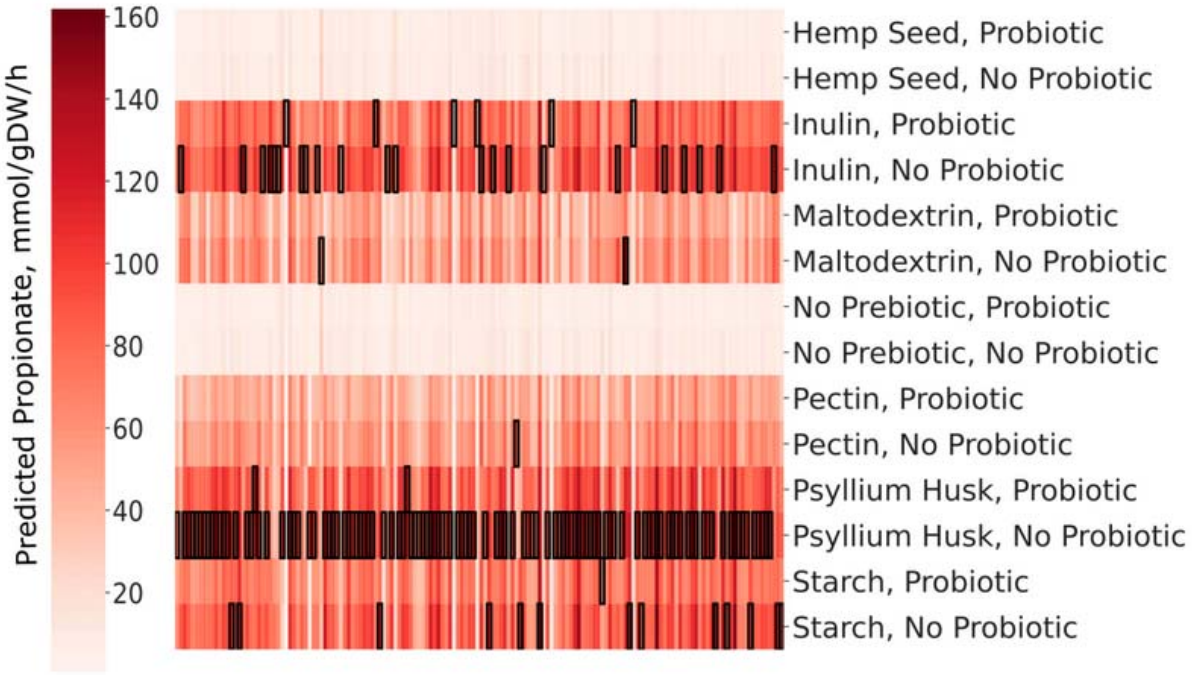

Figure S2. Individual-specific optimal synbiotic treatments for maximizing propionate production. MCMM-predicted propionate production also varied substantially across individuals (N = 156) in response to different synbiotic combinations, though slightly less than for butyrate. The combination of psyllium husk without a probiotic cocktail produced the highest propionate flux in the greatest number of individuals, indicating that the presence of the probiotic strains biases communities away from propionate production, toward butyrate production. However, every other prebiotic/probiotic combination was optimal for at least one individual, with the exceptions of: (1) hemp seed, (2) the no-probiotic condition, (3) maltodextrin with the probiotic cocktail and (4) inulin with the probiotic cocktail. Heatmap colors indicate predicted butyrate flux (mmol/gDW/h), and black boxes denote the most effective treatment for each sample.